Physica C: Superconductivity and its applications 587 (2021) 1353901

Contents lists available at ScienceDirect

Physica C: Superconductivity and its applications

journal homepage: www.elsevier.com/locate/physc

Testing of an MgB_2 coil for a wind turbine generator pole

N. Magnusson [a,*], S.M. Hellesø [a], R. Mikkonen [b], A.B. Abrahamsen [c], M. Runde [a], G. Berg [a], A. Nysveen [d]

[a] SINTEF Energy Research, Trondheim, Norway
[b] Tampere University, Electrical Engineering, Tampere, Finland
[c] DTU Wind Energy, Roskilde, Denmark
[d] Department of Electric Power Engineering, Norwegian University of Science and Technology, Trondheim, Norway

ARTICLE INFO

Keywords:
MgB_2 coil
Wet-winding
Generator pole
Wind power

ABSTRACT

We report on the testing of a 1 m long and 0.5 m wide racetrack coil wound from 4.5 km of MgB_2 tape-shaped superconductors with a copper strip soldered to the nickel matrix. The cross-section of the coil corresponds to what is needed for the field windings of a 10 MW direct drive wind turbine generator pole, but where the straight section has been shortened. Ten double pancake sub-coils were wet-wound, with epoxy as the only electrical insulation, and assembled. The entire coil was cooled down to 14 K, and the direct current was ramped up. Voltage measurements were made over the double pancake coils. For eight of the ten double pancake coils, excessive voltages appeared at currents much lower than the design current. These voltages may either be attributed to the wire quality or to the winding process. A quench was observed at 149 A, which is in reasonable agreement with the predicted load line of the coil obtained by scaling wire transport measurements at 1 T and 20 K with hysteretic magnetization measurements in the range 1-5 T and 5-20 K.

1. Introduction

Intensive development of YBCO [1,2] and MgB_2 [3-5] wires aims at large-scale deployment of superconductors beyond what is economically feasible with low-temperature superconductors, operated at liquid helium temperatures. One, or both, of these wire types may reach commercial performance levels for multiple applications. To define the required wire properties and to demonstrate the potential, work on various applications is needed. Today YBCO conductors are used in cables installed, or to be installed, in the power grid [6,7], and for the development of wind power applications [8]. MgB_2 conductors are used at CERN [9] for current leads to the Large Hydron Collider.

Focusing on the MgB_2 conductor, there are several prospective applications, particularly in the medium magnetic field range of 0.5 – 4 T. Among these are high current cables [10], and coils for magnetic resonance imaging devices [11,12], induction heaters [13], and motors and generators. MgB_2-based motors and generators are considered mainly for ship propulsion [14], electric aircrafts [15,16] and wind turbines.

The motivation for superconducting wind turbine generators is mainly the comparably low volume and weight achievable when increasing the magnetic field in the air gap beyond 1 T [17,18], which is the limit for permanent magnet-based generators. The core technology is the superconducting field coil of the rotor. To assess the technology and to prepare for large-scale industrial production, different winding methods and wires must be examined and tested to obtain reliable coils at a low cost.

Several MgB_2 coils have been manufactured for different purposes, in different sizes and shapes, and using different methods and wires. Small-scale coils have generally been fabricated as a preparational step for larger coils [19-22] or to examine specific topics, like the effects of iron in the conductor matrix [23] or new coil manufacturing methods [24]. Larger coils have been wound to verify the operation under application-like conditions. Two kilometers of MgB_2 wire were wound into a coil with an inner diameter of 0.2 m and tested in external magnetic fields of up to 3 T [25]. In [26], 9 km of Kapton insulated MgB_2 wire was wet-wound into a coil with an inner diameter of 1.1 m, and in [27] 10 km of glass-fiber insulated MgB_2 wire was dry-wound and vacuum impregnated into a coil with an inner diameter of 1.3 m. Aiming at the wind power generator application, a racetrack coil was dry-wound from 3 km of glass-fiber insulated MgB_2 wire [28].

In this article, we report on the testing of a racetrack MgB_2 coil, corresponding to a scaled pole of a 10 MW wind turbine generator.

* Corresponding author.

https://doi.org/10.1016/j.physc.2021.1353901
Received 28 October 2020; Received in revised form 12 February 2021; Accepted 31 May 2021
Available online 2 June 2021

2. MgB_2 coil characteristics

The MgB_2 coil has the same cross-section and coil opening width, and experiences almost the same magnetic field and current as the full scale 10 MW generator pole design described in [29], except for that the straight section of the racetrack-shaped coil, to fit into an existing cryostat and to reduce wire cost, was shortened with a straight section length from 3.1 m to 0.5 m. By scaling the length of the coil only, it will represent a generator with a similar magnet shear force density and thereby demonstrate the MgB_2 coil technology under similar conditions as for a 10 MW direct drive wind turbine generator. The result of reducing the length of the coil for a generator is to reduce the resulting operation torque scaling linear with the length of the straight section. Thus, the MgB_2 coil demonstrator corresponds approximately to a 1.5 MW direct drive wind turbine generator if used with the downscaled dimensions. Fig. 1 shows the design of the MgB_2 demonstration coil, which is wound into the racetrack shape to be incorporated into the rotor of a direct drive wind turbine generator, which will hold between 10-40 of such racetrack coils to provide the magnetic field of the multi-pole generator.

The coil was wound from 4.5 km of tape shaped MgB_2 superconductors (see cross-section in Fig. 2), and built up by stacking ten double pancake coils. The complete coil was 1 m long and 0.5 m wide. The number of turns was 2080, and the design current was 225 A, yielding a maximum magnetic field strength of 2.8 T at the end sections and 2.7 T in the middle of the straight section. The coil was wet-wound using Stycast2850 epoxy resin, which also constituted the turn-to-turn electrical insulation. A mechanical support was applied to the straight section to handle the electromagnetic forces. The fabrication of the coil is described in detail in [30,31]. The main wire and coil characteristics are summarized in Table 1.

The MgB_2 wires were delivered in spools of 500–1000 m and were characterized by the wire manufacturer by measuring the transport critical current of 10 cm long pieces at the beginning and the end of each spool in applied magnetic fields up to 1.8 T and at temperatures of 16–20 K. It was investigated if the critical current, I_c, of the wires could be measured along the length position before winding the pancake coils, but this would have resulted in a test as expensive at purchasing the wire and was therefore discarded. It should be noted that the routinely mapping of I_c of high-temperature superconductors (HTS) using a Tapestar system, where the HTS-tape is rolled through a liquid nitrogen bath while the magnetic field response is measured, does not exist for MgB_2 wires, because it is much more difficult to cool down the MgB_2 below the critical temperature of 39 K.

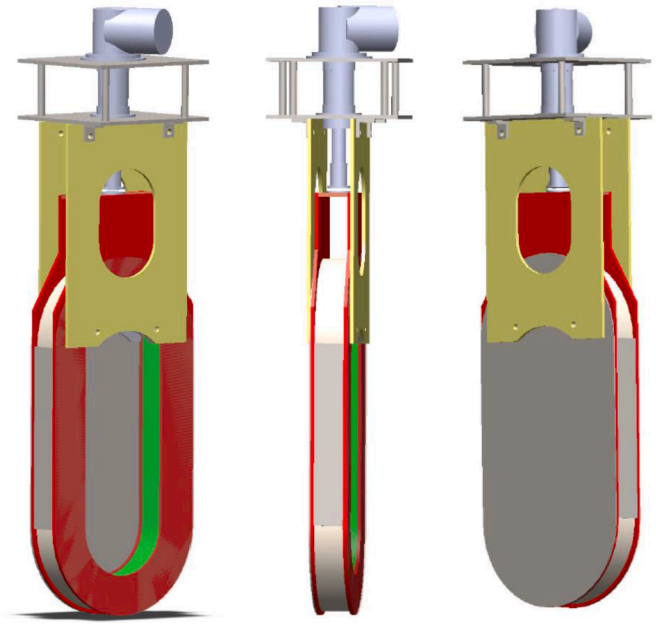

Fig. 1. Schematic layout of the MgB_2 rotor coil demonstrator. The MgB_2 coil (light gray) is wound into the racetrack geometry. The MgB_2 coil is clamped between two copper plates (red) to provide conduction cooling of the coil as provide by the cryocooler cold head mounted at the top. Mechanical support to the straight section of the coil is provide by stainless steel plates and a stainless steel lid (dark gray). The coil assembly is hanging from the top of the radiation shield in two glass fiber plates (yellow).

Fig. 2. Cross-section of the MgB_2 wire composed of MgB_2 filaments (black) embedded in a nickel matrix and with a copper strip soldered on the top.

Table 1
MgB_2 wire and coil characteristics.

Parameter	Description
Superconductor	MgB_2 filaments embedded in nickel matrix with additional copper strip
Wire producer	Columbus Superconductors
Wire dimensions	0.7 mm × 3 mm
Wire critical current	540 A @ 10 K, 1.8 T 230 A @ 20 K, 1.8 T
Coil length	1.0 m
Coil straight section	0.5 m
Coil width	0.5 m
Coil inner opening / end diameter	0.3 m
Coil cross-section (height x width)	81 mm × 87 mm (straight section) 81 mm × 81 mm (end section)
No. double pan-cake coils	10
Total No. turns	2080
Total wire length	4.5 km
Operating temperature	10–20 K
Design current	225 A
Magnetic field, end sections	2.8 T

A second challenge with the MgB_2 wire was that the magnetic field scaling of the critical current was not known for applied magnetic fields above 1.8 T for the specific wires, but only as a general scaling of the type of wire. Thus, to obtain more information about the magnetic field scaling, 3 mm × 3 mm pieces of the different wires were cut and mounted in a 16 T Vibrating sample magnetometer (VSM) from Cryogenic Limited. The magnetization curves of the wires were measured with the magnetic field applied along the normal of the tape face (see Fig. 2) and the hysteretic opening of the magnetization curves, Δm, were derived. When applying the Bean model, Δm becomes proportional to the critical current density, J_c, and one can thereby scale the transport current of a superconducting wire at a reference applied field and temperature to other fields and temperatures using the hysterestic magnetization scaling (see [32] for the scaling method).

Fig. 3 shows the magnetic field and temperature scaling of the MgB_2 wire as provided by the manufacturer in applied magnetic fields up to 1.8 T as well as the expected scaling at higher applied magnetic field as determined from the hysteretic opening of the magnetization curves [33]. The transport measurement at 1 T and 20 K has been used as the reference point of the magnetization scaling and it can be seen that there is reasonable correspondence between the transport and magnetization scaling as function of magnetic field at 20 K. At 16 K the magnetization scaling seems to fall off faster towards higher magnetic field than for the transport measurements. Finally, the loadline showing the maximum magnetic field produced inside the MgB_2 demonstration coil when

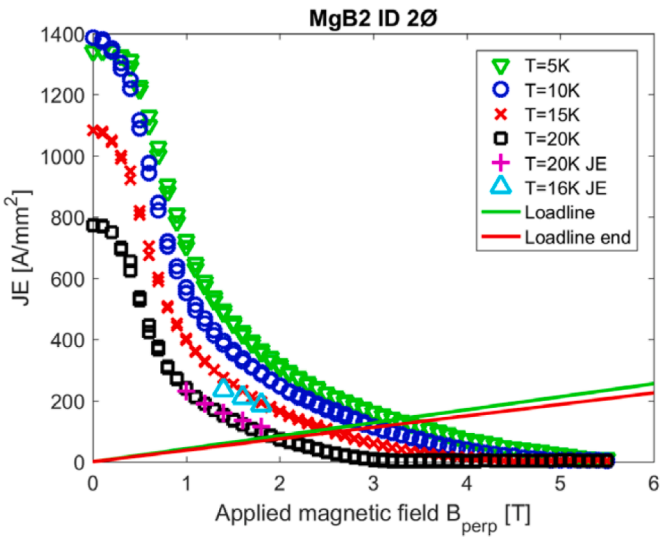

Fig 3. Scaling of the engineering current density J_E of the MgB_2 wires used for the MgB_2 demonstration coil as determined from transport measurements indicated by label "JE" as provided by the wire manufacturer. The hysteretic opening of the magnetization curves has been used to scale the transport current density at 1 T and 20 K to operation temperatures between 5 and 20 K and applied fields up to 5.5 T. The loadlines of the MgB_2 demonstration coil are added as solid lines for the straight section (green) and for the racetrack end winding (red). Reproduced from [33].

ramping up the current of the coil is shown for both the straight and the end section of the coil. The load line has been determined by repeating the analysis of [29] on the shorter coil. The transition out of the superconducting state is expected when the load lines are crossing the critical engineering current density of the MgB_2 wires and Table 2 shows the expected safe operation of the demonstration coil for operation temperatures between 5 and 20 K. It is clearly seen that the original design target field of $B = 2.8$ Tesla in [29] will demand an operation temperature around 10 K due to the somewhat lower wire specifications compared to the initial MgB_2 properties used to the 10 MW generator design.

3. Cooling

The coil was tested in a slightly modified cryostat previously used for a circular MgB_2 coil [34]. A two-stage Gifford-McMahon cryocooler was used. The cold head of the second stage, providing 15 W cooling power at 20 K, was thermally connected to a copper interface glued to the coil using Stycast2850. To allow for different thermal expansion of the support holding the coil and the thermal connection, 1 mm thick copper plates were used yielding some flexibility, see Fig. 4. The coil, the thermal interface, and the support handling electromagnetic forces hung vertically in fiber-glass reinforced epoxy plates, fastened to a rigid top plate. A decagonal copper thermal radiation shield clad with 30 layers of superinsulation surrounded the coil (the sides, but not the back and front plates, of the structure are shown in Fig. 5) and was thermally connected to the first stage of the cold head with a cooling power of 80 W at 80 K. The system was placed in vacuum in a stainless-steel cryostat.

Table 2
Safe operational current of the MgB_2 demonstration coil determined from scaling of the critical current of the MgB_2 wire and the loadline of the coil. The safe engineering current density of the wire is defined at 25% below the critical engineering current density. Reproduced from [33].

T [K]	$J_{E,\ critical}$ [A/mm^2]	$J_{E,\ safe}$ [A/mm^2]	$B_{critical}$ [T]	$I_{operation,\ safe}$ [A]
5	158	119	3.4	332
10	142	107	3.0	298
15	116	87	2.5	183
20	83	62	1.9	130

The current leads were designed for 250 A. Between room temperature and the first stage, brass leads were used, optimized with an IL/A ratio of 6.5×10^5 A/m derived from [35], where I is the current, L the length and A the cross-section of the lead. Between the first stage and the coil, BSCCO/Ag high-temperature superconducting (HTS) tapes were used. Three tapes were connected in series with their faces in parallel to the magnetic field to limit the field dependent reduction of the critical current. At 0.2 T and 66 K (the design value at the top of the current leads), the critical current per tape was 120 A.

The HTS tapes were soldered, with a 10-cm overlap, to the MgB_2 conductors of the two outer double pancake coils. The same overlap was used for the soldering of the MgB_2 conductors between the double pancake coils. To efficiently remove the heat generated in the joints, they were on both sides thermally anchored to copper plates connected to the thermal interface, as shown in Fig. 4.

Before the cooling machine was switched on, the cryostat was evacuated to 10^{-4} mbar using a turbomolecular vacuum pump. The cool-down sequence of the coil is shown in Fig. 6. The coil reached an operating temperature of 14 K in four days, and measurements commenced after five days. The temperature of the first stage was then approximately 50 K.

4. Quench protection

A simple quench protection scheme was applied, see Fig. 7. A bridge circuit measuring the voltage, U_1, between the center of the MgB_2 coil (L) and in between two resistances (R_3 and R_4), where one of the resistances is variable and that resistance is adjusted such that U_1 is practically zero under normal ramping. If U_1 rises to above 0.05 V, due to an imbalance between the halves of the coil, the switch opens. Such an imbalance is likely caused by a quench, and then the energy stored in the coil is dissipated partly in the coil and partly in the shunt resistor, R_2. A standard power supply was used, which worked best in controlled voltage mode. The resistor R_1 stabilizes the current by adding resistance to the circuit, and it allows for a power dissipation outside the power source when the current is ramped down.

Responses to manually closures of the switch are shown in Fig. 8 for three currents. The energies released were 6.2 kJ, 8.8 kJ and 20.3 kJ at 52 A, 62 A and 94 A, respectively. Approximately 80% of the energy was released within 30 s for all cases.

5. Coil current-voltage characteristics

Current was injected into the coil with a ramping rate of approximately 0.05 A/s. As a voltage source was used, a duration of 15-20 minutes was necessary at each current level for the current to stabilize and the inductive voltages over the coils to reach an acceptable level.

Voltages were measured over the double pancake coils individually. In most of the coils, voltages appeared at rather low currents. Fig. 9 shows the voltage over pancake coils 3, 4, 5, 7 and 9, numbered from one side to the other, and Fig. 10 shows the voltages for the double pancakes 1, 2, 6, 8 and 10 (note the different scales on the voltage axes). As can be seen, only double pancake coils 4 and 5 showed voltages, which were within the uncertainty of the induced inductive voltages due to small variations in current ($dI/dt = 20$ μA/s yields a voltage of 10 μV for one double pancake coil).

The voltages appearing resulted in a comparably high power dissipation, 2.1 W for the full coil at 140 A. The measured temperature (at the outside of the coil) increased approximately three degrees during the measurement sequence, from 14 K to 17 K, for measurements up to 140 A. At 149 A the coil quenched.

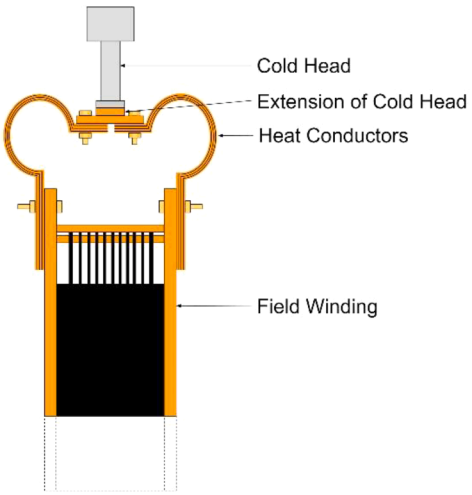

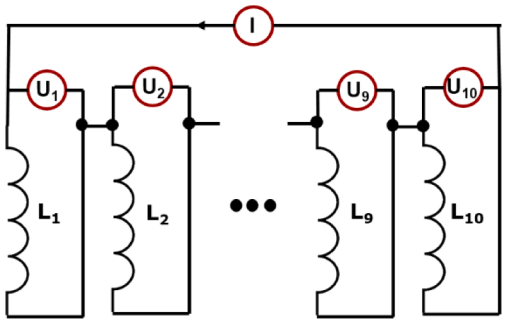

Fig. 4. Left: Schematic drawing of the top of the coil (black) and the thermal interface with its connection to the cold head. The double pan-cakes no. 1-10 are positioned next to each other from left to right. The 10 black stripes at the top of the coil represents the end wires of the double pancakes. The two horizontal copper plates in the center cool the soldered joints between double pancakes. Right: Serial connection diagram for the 10 double pancake coils and the measurement of the individual coil voltages.

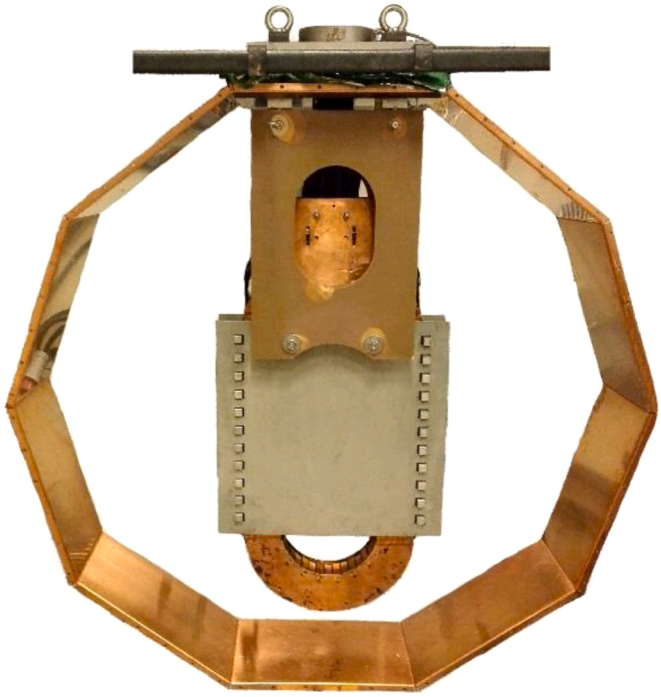

Fig. 5. The coil hangs vertically in one fiber-glass reinforced epoxy plate on each side (one shown with the large oval hole on the photo). The square grey stainless-steel plates (one on each side) handle the coil's electromagnetic forces. The decagonal outer structure is a part of the first stage thermal shield.

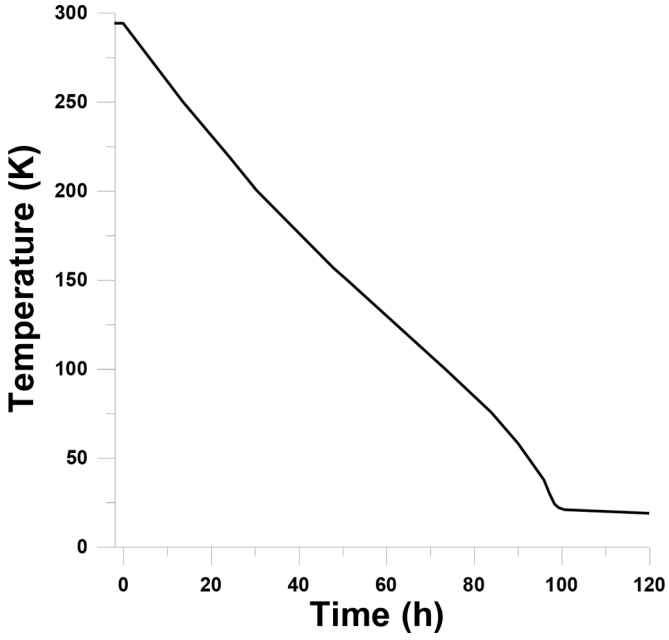

Fig. 6. Cool-down sequence for the coil, from room temperature to approximately 14 K.

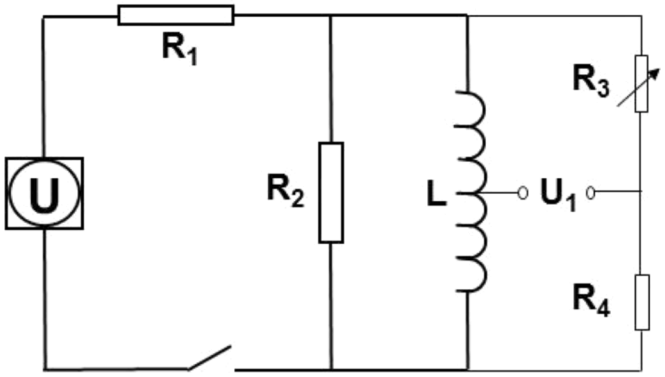

Fig. 7. Quench protection circuit. The MgB_2 coil, L, has an inductance of 4.6 H, R_1 is 0.02 Ω, R_2 0.85 Ω, and R_3 and R_4 100 Ω.

6. Discussion

The rather large voltages appearing in some of the double pancake coils at currents far below the expected, indicate that there are regions where a substantial amount of the current is carried by the copper strip (and nickel matrix, but as the matrix resistance is significantly higher than the copper strip resistance, we neglect it). The coil with the largest voltage drop in Fig. 10 showed an onset of voltage at 20–30 A, followed by increasing voltages as the current was raised. For high currents, the current-voltage behavior is close to linear. This behavior may be explained by that there are regions in the MgB_2 tape with different degrees of damaged filaments. The first voltage appearing, originates in a region with a critical current in the 20–30 A range. As the current is increased, there are regions with higher (but still low) critical current

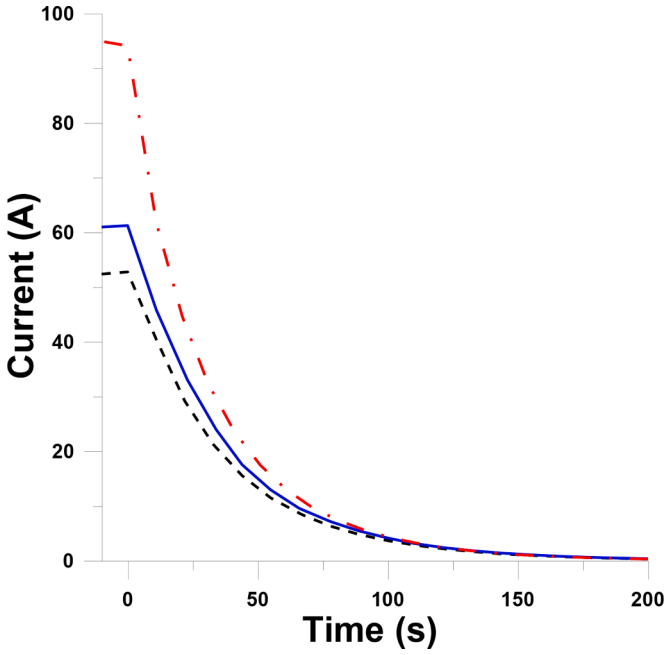

Fig. 8. Examples of current decay when triggering the quench protection at 52, 62 and 94 A.

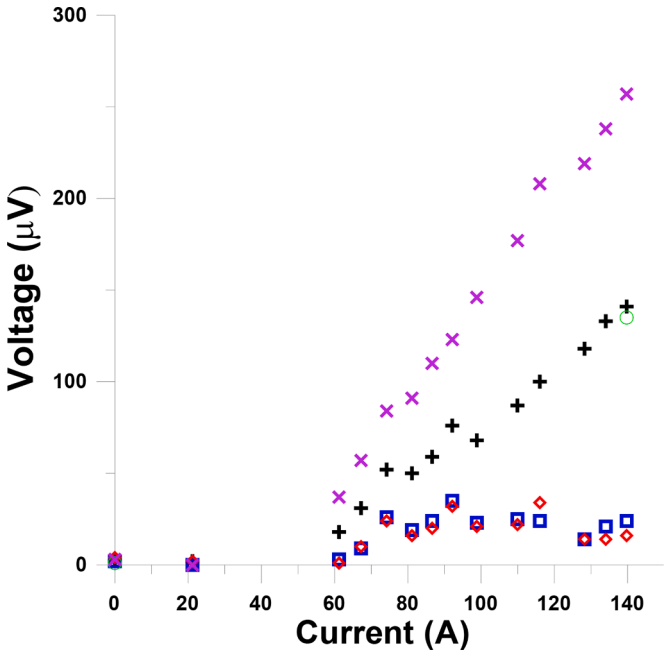

Fig. 9. Voltages appearing over double pancake coils 3 (+), 4 (□), 5 (◊), 7 (○) and 9 (x), measured at approximately 15 K. The voltage of double pancake coil 7 was only measured at 140 A.

where the current is pushed out into the copper strip. When entering the linear behavior for currents above approximately 110 A, there are no further regions with low critical current (at least not with critical current below 146 A), and all additional current is carried by the copper strip. Fig. 11 shows a simple wire model to represent the total wire measurement of such different segments.

By determining the slope of the *I-V* curves at high currents in Figs. 9 and 10 as dU/dI, the resistance and thereby the length of the wire with low critical current can be estimated as illustrated in Fig. 11. For the double pancake coil with the highest voltage, the additional current,

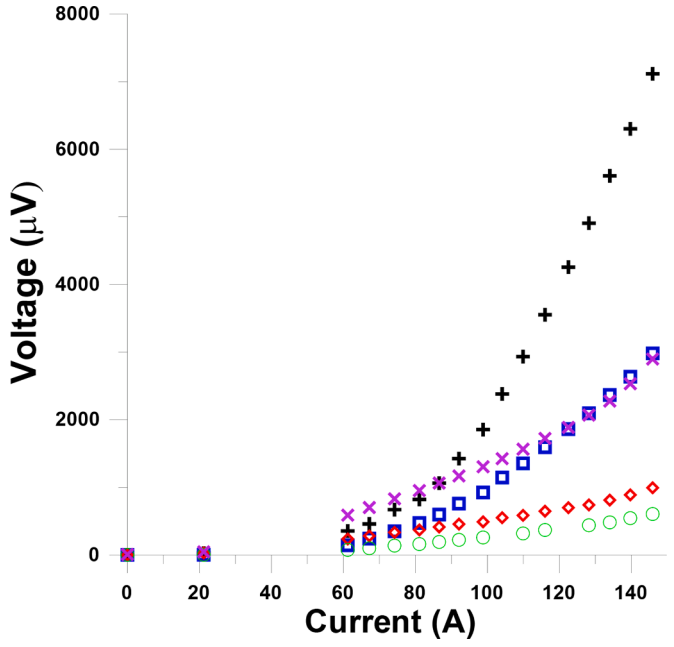

Fig. 10. Voltages appearing over double pancake coils 1 (+), 2 (□), 6 (◊), 8 (○) and 10 (x), measured at approximately 15 K.

which was not carried by the superconducting filaments, sees a resistance of dU/dI ~ 120 μΩ, which corresponds to approximately 1.2 m of the conductor, since the copper strip has a specific resistance of 100 μΩ/m at 15 K. The corresponding exercises were made for the other double pancake coils, using the slope of the *I-V* curves at 140 A when there was no clear linear region for the voltage (corresponding to that there were still regions with critical current in the 130–150 A range). The slopes and the resulting length of the weak wire segments are given in Table 3.

Several possible reasons exist for the low critical currents of 30 A in parts of the wire. It could be due to the quality of the wire, the winding process, the cooling, or the electromechanical forces. The two latter may be considered unlikely, as the current-voltage characteristics stayed the same as the coil was both cycled in temperature and in current. Although precautions were taken for the coil winding, including pulling force stabilizers for the wire, it cannot be ruled out that stresses on the wire have been too high in one or more of the coil manufacturing steps. A critical step in that process is the manual handling of the spools when going from the lower to the upper layer of a double pancake coil. It is also possible that the particular wire used suffered from quality issues with some regions with lower critical current than others, but this remains unknown as characterization along the length of the wire was not practically feasible.

The coil was wound without dedicated electrical insulation, yielding high thermal conductivity between turns, and could therefore be run with a local power dissipation which otherwise would have led to a quench at much lower currents. Nevertheless, the quench occurred at currents much lower than expected from the short sample critical current data and at only two thirds of the design current. It should however be noted that the temperature of the coil increased due to the heat dissipation in the weak superconducting pancake coils from about 14 K to about 17 K before the quench occurred at 149 A. By comparing this increased operation temperature to Table 2 it is seen that safe operation is predicted to be between 130 and 183 A for temperatures between 15 and 20 K. It is quite likely that that the local temperature of the coil has been higher than 17 K, whereby the observation of a quench at 149 A is in fairly good agreement with the predictions of Fig. 3 and Table 2. One could argue that the capability of the good regions of the coil was not fully tested, but testing of parts of the pancake coils is simply not doable

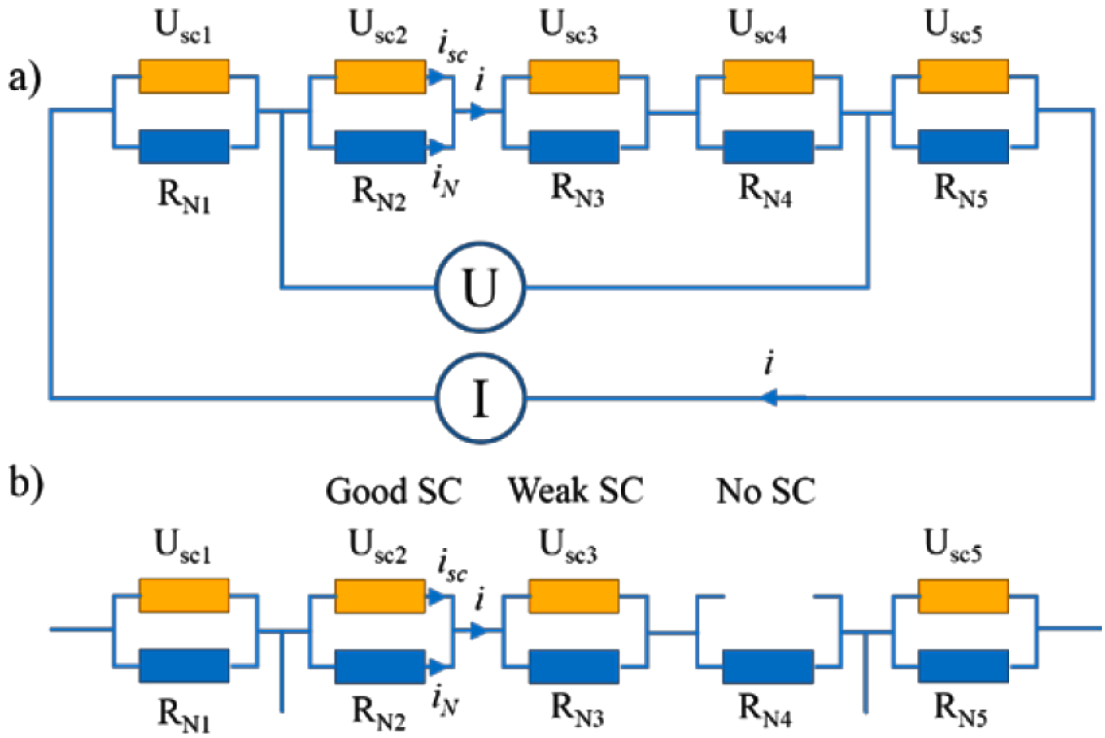

Fig. 11. a) Illustration of a wire model as composed of superconducting elements coupled in parallel with a normal resistor representing the nickel matrix and the copper strip soldered to the MgB_2 wire. The voltage and current across the superconductor winding was measured with a 4-point measurement setup. **b)** Illustration of a wire where the segment U_{sc2} has a high critical current, U_{sc3} has a low critical current and the segment U_{sc4} is not superconducting at all. The total wire voltage thereby becomes the sum of the different elements, which will result in current sharing if the current of the wire is above the critical current of the segments. Reproduced from [36].

Table 3
Approximate resistances and lengths of normal zones for the ten double pancake coils at 140 A.

Coil No.	$R = dU/dI$ (μΩ)	Normal zone (m)
1	120	1.2
2	57	0.57
3	2	0.02
4	0	0
5	0	0
6	15	0.15
7[a]	N.A.	N.A.
8	9	0.09
9	3	0.03
10	54	0.54

[a] The voltage of coil No. 7 was only measured at 140 A.

due to the geometry and that the coils are glued together with epoxy and inseparable without damaging of the coils.

The absence of a quench although meter-long parts of the coil was operated above the critical current with a resulting joule heating of the matrix and copper strip of up to 2 W demonstrates good cooling capabilities of the coil. The winding without dedicated electrical insulation (and thereby thermal insulation) largely enhance the thermal conductivity between turns and allows for operation of the coil although short parts of the wire is operated above its local critical current.

Important motivations for the fabrication of the coil were to test the winding method as well as the mechanical support method. With the observed voltage drops in the wire for the reasons given above, the results are inconclusive as regards the quality of the winding and support methods. It cannot be ruled out that some damage has occurred after the wire was received or that some damages would appear at higher currents, due to higher electromagnetic forces. However, the two coils practically without voltage drops up to 140 A show that it is possible to successfully wind MgB_2 double pancake coils with the method used.

7. Conclusions

The tested MgB_2 coil showed excessive voltage drops in eight out of ten sub-coils at currents much lower than the design current. The absence of dedicated electrical insulation; which lowered the thermal insulation of the coil; allowed the coil to operate at a power dissipation of above 2 W before it quenched at 149 A. The observed quench current is in fairly good agreement with the loadline predicted from magnetization measurements scaling of the critical current of the wire, when it is taken into account that the operation temperature of the coil was increased from about 14 to 17 K before the quench occurred due to the increased heat dissipation in the weak segments of the MgB_2 wire.

CRediT authorship contribution statement

N. Magnusson: Conceptualization, Methodology, Formal analysis, Investigation, Writing - original draft, Writing - review & editing, Visualization, Funding acquisition. **S.M. Hellesø:** Formal analysis, Investigation, Writing - review & editing, Visualization. **R. Mikkonen:** Methodology, Writing - review & editing, Resources. **A.B. Abrahamsen:** Conceptualization, Methodology, Writing - review & editing, Visualization, Funding acquisition. **M. Runde:** . **G. Berg:** Investigation. **A. Nysveen:** Supervision.

Declaration of Competing Interest

The authors declare that they have no known competing financial interests or personal relationships that could have appeared to influence the work reported in this paper.

Acknowledgments

This work has been done as part of the INNWIND.EU project funded by the European Community's Seventh Framework Programme under grant agreement No. 308974 (INNWIND.EU) and the NOWITECH programme funded by the Research Council of Norway under contract No.193823.

References

[1] A. Sundaram, Y. Zhang, A.R. Knoll, D. Abraimov, P. Brownsey, M. Kasahara, G. M. Carota, R. Nakasaki, J.B. Cameron, G. Schwab, L.V. Hope, R.M. Schmidt, H. Kuraseko, T. Fukushima, D.W. Hazelton, 2G HTS wires made on 30 μm thick Hastelloy substrate, Supercond. Sci. Technol. 29 (2016), 1004007.

[2] S. Lee, V. Petrykin, A. Molodyk, S. Samoilenkov, A. Kaul, A. Vavilov, V. Vysotsky, S. Fetisov, Development and production of second generation high Tc superconducting tapes at SuperOx and first tests of model cables, Supercond. Sci. Technol. 27 (2014), 044022.

[3] M. Tropeano, A. Ballarino, C. Bruzek, G. Escamez, S. Giannelli, K. Konstantopoulou, F. Lesur, A. Marian, G. Grasso, MgB_2 Round Wires for the High-Power Superconducting Cable Demonstrator in the Best Paths Project, presented at EUCAS2017, Geneva, 2017, pp. 17–21.

[4] F. Wan, M.D. Sumption, M.A. Rindfleisch, M.J. Tomsic, E.W. Collings, Architecture and transport properties of multifilamentary MgB_2 strands for MRI and low AC loss applications, IEEE Trans. Appl. Supercond. 27 (2017), 7755738.

[5] M. Kodama, T. Suzuki, H. Tanaka, K. Okishiro, K. Okamoto, G. Nishijima, A. Matsumoto, A. Yamamoto, J. Shimoyama, K. Kishio, High-performance dense MgB_2 superconducting wire fabricated from mechanically milled powder, Supercond. Sci. Technol. 30 (2017), 044006.

[6] H. Yumura, Y. Ashibe, H. Itoh, M. Ohya, M. Watanabe, T. Masuda, C.S. Weber, Phase II of the Albany HTS cable project, IEEE Trans. Appl. Supercond. 19 (2019), 5067112.

[7] S.H. Sohn, H.S. Yang, J.H. Lim, S.R. Oh, S.W. Yim, S.K. Lee, H.M. Jang, S. D. Hwang, Installation and power grid demonstration of a 22.9 kV, 50 MVA, high temperature superconducting cable for KEPCO, IEEE Trans. Appl. Supercond. 22 (2012), 5800804.

[8] A. Bergen, R. Andersen, M. Bauer, H. Boy, M. ter Brake, P. Brutsaert, C. Bührer, M. Dhallé, J. Hansen, H. ten Kate, J. Kellers, J. Krause, E. Krooshoop, C. Kruse, H. Kylling, M. Pilas, H. Pütz, A. Rebsdorf, M. Reckhard, E. Seitz, H. Springer, X. Song, N. Tzabar, S. Wessel, J. Wiezoreck, T. Winkler, K. Yagotyntsev, Design and in-field testing of the world's first ReBCO rotor for a 3.6 MW wind generator, Supercond. Sci. Technol. 32 (2019), 125006.

[9] A. Ballarino, Development of superconducting links for the Large Hadron Collider machine, Supercond. Sci. Technol. 27 (2014), 044024.

[10] A. Ballarino, C.E. Bruzek, N. Dittmar, S. Giannelli, W. Goldacker, G. Grasso, F. Grilli, C. Haberstroh, S. Holé, F. Lesur, A. Marian, J.M. Martínez-Val, L. Martini, C. Rubbia, D. Salmieri, F. Schmidt, M. Tropeano, The BEST PATHS project on MgB2 superconducting cables for very high power transmission, IEEE Trans. Appl. Supercond 26 (2016), 7438787.

[11] M. Razeti, S. Angius, L. Bertora, D. Damiani, R. Marabotto, M. Modica, D. Nardelli, M. Perrella, M. Tassisto, Construction and operation of cryogen free MgB_2 magnets for open MRI systems, Supercond. Sci. Technol. 18 (2008) 882–886.

[12] T. Baig, Z. Yao, D. Doll, M. Tomsic, M. Martens, M, Conduction cooled magnet design for 1.5T, 3.0T and 7.0T MRI systems, Supercond. Sci. Technol. 27 (2014), 125012.

[13] N. Magnusson, M. Runde, A 200 kW MgB_2 induction heater project, J. Phys.: Conf. Ser. 43 (2006) 1019–1022.

[14] P.C. Michael, J. Kvitkovic, S.V. Pamidi, P.J. Masson, L. Bromberg, Development of MgB2-cabled conductors for fully superconducting rotating electric machines, IEEE Trans. Appl. Supercond. 27 (2017), 7833171.

[15] F. Berg, J. Palmer, P. Miller, M. Husband, G. Dodds, HTS electrical system for a distributed propulsion aircraft, IEEE Trans. Appl. Supercond. 25 (2015), 5202705.

[16] C.D. Manolopoulos, M.F. Iacchetti, A.C. Smith, K. Berger, M. Husband, P. Miller, Stator design and performance of superconducting motors for aerospace electric propulsion systems, IEEE Trans Appl. Supercond. 28 (2018), 5207005.

[17] A.B Abrahamsen, D. Liu, N. Magnusson, A. Thomas, Z. Azar, E. Stehouwer, B. Hendriks, G.J. van Zinderen, F. Deng, Z. Chen, D. Karwatzki, A. Mertens, M. Parker, S. Finney, H. Polinder, Comparison of levelized cost of energy of superconducting direct drive generators for a 10 MW offshore wind turbine, IEEE Trans. Appl. Supercond. 28 (2018), 5208205.

[18] S. Sanz, T. Arlaban, R. Manzanas, M. Tropeano, R. Funke, P. Kovác, Y. Yang, H. Neuman, B. Mondesert, Superconducting light generator for large offshore wind turbines, J. Phys. Conf. Ser. 507 (2014), 032040.

[19] M. Runde, A. Stenvall, N. Magnusson, G. Grasso, R. Mikkonen, MgB_2 coils for a DC superconducting induction heater, J. Phys.: Conf. Ser. 97 (2008), 012159.

[20] S. Mine, M. Xu, S. Buresh, W. Stautner, C. Immer, E.T. Laskaris, K. Amm, G. Grasso G, Second test coil for the development of a compact 3 T MgB_2 magnet, IEEE Trans. Appl. Supercond. 23 (2013), 6376127.

[21] R. Pasquet, C. Berriaud, F. Forest, C. Hilaire, F.P. Juster, A. Porhiel, T. Schild, L. Scola, A. Taleb, Design and test of a small react-and-wind MgB2 double pancake, IEEE Trans. Appl. Supercond. 25 (2015), 4603605.

[22] H.S. Kim, C. Kovacs, M. Rindfleisch, J. Yue, D. Doll, M. Tomsic, M.D. Sumption, E. W Collings, Demonstration of a conduction cooled react and wind MgB2 coil segment for MRI applications, IEEE Trans. Appl. Supercond. 26 (2016), 4400305.

[23] X.H. Li, X.J. Du, M. Qiu, Y.W. Ma, L.Y. Xiao, Design and experimental demonstration of an MgB_2 based 1.5 T MRI test magnet, Physica C 463-465 (2007) 1338–1341.

[24] C. Hori, R. Nakagawa, Y. Imamura, H. Tanaka, Development of a test conduction-cooled MgB_2 Coil, IEEE Trans. Appl. Supercond. 26 (2016), 4901004.

[25] M. Kazazi, C. Berriaud, C. Hilaire, F.P. Juster, R. Pasquet, T. Schild, Design, manufacture, and tests of a 1+3 Teslas MgB_2 dry magnet, IEEE Trans. Appl. Supercond. 27 (2017), 4601905.

[26] F. Sætre, I. Hiltunen, M. Runde, N. Magnusson, J. Järvelä, J. Bjerkli, E. Engebrethsen, Winding, cooling and initial testing of a 10 H superconducting MgB2 coil for an induction heater, Supercond. Sci. Technol. 24 (2011), 035010.

[27] M. Modica, S. Angius, L. Bertora, D. Damiani, M. Marabotto, D. Nardelli, M. Perrella, M. Razeti, M. Tassisto, Design, construction and tests of MgB2 coils for the development of a cryogen free magnet, IEEE Trans. Appl. Supercond. 17 (2007) 2196–2199.

[28] G. Sarmiento, S. Sanz, A. Pujana, J.M. Merino, I. Marino, M. Tropeano, D. Nardelli, G. Grasso, Design and testing of real-scale MgB_2 coils for suprapower 10-MW wind generator, IEEE Trans. Appl. Supercond. 26 (2016), 7397945.

[29] A.B. Abrahamsen, N. Magnusson, B.B. Jensen, D. Liu, H. Polinder, Design of an MgB_2 race track coil for a wind generator pole demonstration, J. Phys. Conf. Ser. 507 (2014), 032001.

[30] N. Magnusson, J.C. Eliassen, A.B. Abrahamsen, A. Nysveen, J. Bjerkli, M. Runde, P. King, Design aspects on winding of an MgB_2 superconducting generator coil, Energy Procedia 80 (2015) 56–62.

[31] N. Magnusson, J.C. Eliassen, A.B. Abrahamsen, S.M. Hellesø, M. Runde, A. Nysveen, L.E. Moslått, J. Bjerkli, P. King, Fabrication of a scaled MgB_2 racetrack demonstrator pole for a 10 MW direct drive wind turbine generator, IEEE Trans. Appl. Supercond. 28 (2018), 5207105.

[32] A.B. Abrahamsen, B.B. Jensen, E. Seiler, N. Mijatovic, V.M. Rodriguez-Zermeno, N. H. Andersen, J. Østergård, Feasibility study of 5 MW superconducting wind turbine generator, Physica C 471 (2011) 1464–1469.

[33] N. Magnusson, S.M. Hellesø, M.E. Paulsen, J.C. Eliassen, A.B. Abrahamsen, Fabrication of MgB2 Coils – A superconducting generator pole demonstrator, Deliverable D3.13 of the INNWIND.EU project, 2016.

[34] I. Hiltunen, A. Stenvall, A. Korpela, J. Lehtonen, R. Mikkonen, M. Runde, N. Magnusson, G. Kalkowski, Cryogenic design of the Aluheat project, AIP Conf. Proc. 985 (2008) 1015–1022.

[35] Seeber H 1998 Handbook of Applied Superconductivity Institute of Physics Publishing, Bristol.

[36] A.B. Abrahamsen, D. Liu and H. Polinder, Direct drive superconducting generators for INNWIND.EU wind turbines, Deliverable D3.11 of the INNWIND.EU project (2018).